CARBON 75 (2014) 345–352

Available at www.sciencedirect.com

ScienceDirect

journal homepage: www.elsevier.com/locate/carbon

Synthesis of carbon nanotube/mesoporous TiO_2 coaxial nanocables with enhanced lithium ion battery performance

Lifang He [a,*], *Chundong Wang* [c], *Xiaolin Yao* [a], *Ruguang Ma* [c], *Hongkang Wang* [c], *Peirong Chen* [a], *Kui Zhang* [b,*]

[a] *Department of Applied Chemistry, Anhui Agricultural University, Hefei 230036, China*
[b] *Institute of Intelligent Machines, Chinese Academy of Sciences, Hefei, Anhui 230031, China*
[c] *Center of Super-Diamond Advanced Films (COSDAF), City University of Hong Kong, Hong Kong, China*

ARTICLE INFO

Article history:
Received 17 December 2013
Accepted 5 April 2014
Available online 13 April 2014

ABSTRACT

Well-organized hybrid nanocables consisting of carbon nanotube (CNT) core and mesoporous TiO_2 sheath has been synthesized through a combined sol–gel and hydrothermal process. By using hexadecylamine as a structure directing agent, mesoporous TiO_2 with thickness ranging from 40 to 70 nm was uniformly deposited on multi-walled CNTs. The resultant one dimensional CNT core/mesoporous TiO_2 sheath (CNT@mesoporous TiO_2) hybrid nanocables shows well-crystallized quality, porous feature and large surface area, favoring its electrochemical performance. Compared with reference TiO_2 without CNTs, the CNT@mesoporous TiO_2 hybrid nanocables shows largely enhanced rate performance, which could be attributed to its unique structure as well as the improvement of electronic conductivity by adding conductive CNTs.

1. Introduction

TiO_2 has stimulated tremendous interests due to its wide potential applications in various fields, such as photocatalysis, sensing, energy storage, solar cell, etc. [1–5]. For the application in lithium ion battery (LIB), TiO_2 has been viewed as one promising alternative to traditional carbonaceous anodes because of its low cost, abundance, stability and nontoxicity. More importantly, TiO_2 exhibits a relatively high lithium insertion/extraction voltage, which helps to avoid the formation of solid-electrolyte interphase layers and lithium electroplating [6], leading to safer anodes with better cycling performance compared with that of graphite. However, TiO_2 also has an intrinsic drawback; it has poor lithium ionic and electrical conductivity. Thus, coarse TiO_2 often shows unsatisfactory rate performance [7,8].

Many efforts have been taken to overcome the above issue [9–12]. Firstly, synthesizing nanosized TiO_2 materials with short path lengths for lithium ions can improve the low ionic conductivity in some extent [13]. For example, TiO_2 nanocrystals, nanowires, and nanotubes have been prepared with higher capacity and better capacity retention in comparison with that of bulk TiO_2 materials [14–16]. Nanostructured TiO_2 materials with porous structure may also yield additional advantages. Mesoporous TiO_2 is a remarkable example and offers important benefits: (1) nanosized TiO_2 crystals as well as mesopores provide short path lengths for fast lithium ions transfer, enabling battery to use materials with improved

* *Corresponding authors.*
E-mail address: kzhang@iim.ac.cn (K. Zhang).
http://dx.doi.org/10.1016/j.carbon.2014.04.013
0008-6223/

ionic conductivity; (2) the large surface area facilitates the access of the electrolyte within the whole electrode and increases electrode/electrolyte contact area, resulting in higher utilization of active materials. For these reasons, mesoporous TiO_2 always exhibits excellent electrochemical performance [17–21]. Secondly, to improve the electronic conductivity of TiO_2-based electrodes, conductive additives including various metals, metal oxides and carbonaceous materials have been integrated within TiO_2 [22–24]. Among them, carbon nanotube (CNT) with superior electrical conductivity, large surface-to-volume ratio, and excellent mechanical and chemical stability has attracted much attention [25,26]. Hybrid materials composed of CNT and nanosized electroactive materials are suitable for LIB [27–29]. Thus, it is expected that decorating mesoporous TiO_2 onto conductive CNTs substrate could improve the LIB performance of TiO_2 by combining the advantages of mesoporous structure and enhanced electronic conductivity.

Various methods have been employed for the synthesis of CNT/TiO_2 composites, including mechanical mixing, chemical vapor deposition and electro-spinning approaches [30–32]. However, these techniques are somehow complicated and require specialized equipment. Sol–gel synthesis is the most common and preferred method to fabricate the binary composite, but the resultant composite always shows phase separation between surface TiO_2 and underneath CNT, leading to uncontrollable growth of TiO_2 particles [33,34]. Recently, only several works reported the uniform deposition of TiO_2 layer on CNT can be achieved [35–41]. However, in the nanoscale, the controllable growth of porous TiO_2 building blocks on CNT is still a challenge.

Herein, we have developed an effective method to coat uniform mesoporous TiO_2 onto CNT scaffold. The synthesis process consists of a sol–gel method combined with a hydrothermal treatment and a short post-annealing procedure. The uniform one dimensional (1D) CNT core/mesoporous TiO_2 sheath (CNT@mesoporous TiO_2) hybrid nanocables was characterized by kinds of techniques and employed as an anode material for LIBs. The results indicate that the hybrid nanocables exhibited excellent electrochemical performance in terms of capacity, stability, and reversibility, even at high charge/discharge rates.

2. Experiment

2.1. Materials

Hexadecylamine (HDA, ⩾90%), tetrabutyl titanate (TBOT, ⩾97%), multi-walled CNTs (MWCNTs, 40–60 nm in diameter, Shenzhen Nanotech Port Co. Ltd.), concentrated nitric acid (HNO_3, 65%) and absolute ethanol (⩾99.8%) were used in the synthesis. CNTs were firstly refluxed in 6 M HNO_3 solution to remove impurities.

2.2. Synthesis of CNT@mesoporous TiO_2 hybrid nanocables

The CNT@mesoporous TiO_2 hybrid nanocables were synthesized according to a previous report with some modification [42]. In a typical synthesis, the acid-treated CNTs (20 mg), 500 μL of deionized (DI) water and 0.6 g of HDA were ultrasonically dispersed in 50 mL of absolute ethanol for 4 h. Then 400 μL (400 mg) of TBOT was slowly added in the mixture under vigorous magnetically stirring. After being further stirred for about 10 min, the mixture was kept static for 8 h at room temperature. The black precipitate was then collected by centrifugation, washed with absolute ethanol, and dried at 60 °C. A hydrothermal process was used to crystallize the amorphous TiO_2. 0.8 g of the above dried powder was dispersed in a solution of 10 ml ethanol and 5 ml DI water. The resultant mixture was sealed within a Teflon-lined autoclave (20 ml) and heated at 180 °C for 12 h. The product was collected by centrifugation and washed with ethanol and DI water. Finally, the dried powder was calcined at 500 °C for 2 h under N_2 to remove organic components. The reference TiO_2 powder was prepared by the similar procedure but without the addition of CNT.

2.3. Characterization

The as-prepared samples were characterized by scanning electron microscopy (SEM, Philips XL 30FEG) and transmission electron microscopy (TEM, Philips CM 20 FEG TEM operated at 200 kV). The X-ray diffraction (XRD) patterns were recorded using Philips X'Pert MRD X-ray diffractometer with Cu Kα radiation. Thermal gravimetric analysis (TGA) was conducted on a TA instrument (TGAQ50, TA USA) from room temperature to 700 °C at a heating rate of 10 °C/min under air atmosphere. Raman measurement was obtained with a Renishaw inVia Raman microscope with 514 nm wavelength. The specific surface area and pore size distribution of the samples were determined by nitrogen adsorption–desorption isotherms at 77 K using a NOVA1200e Surface Area & Pore Size Analyzer (Quantachrome Instruments). Prior to adsorption experiments, the samples were degassed for 2 h at 100 °C.

The working electrodes were prepared by mixing 80 wt.% active materials, 10 wt.% Super P and 10 wt.% poly(vinylidene fluoride) binder dissolved in N-methylpyrrolidone solution. The resultant slurry was then uniformly coated on a copper foil current collector and dried overnight under vacuum. The cells were assembled in an argon filled glove box using a lithium metal foil as the counter-electrode and a Celgard 2400 microporous poly-propylene membrane as the separator. Galvanostatic electrochemical experiments were carried out with a model BT 200 battery cycler (Arbin Instruments, College Station, TX) at room temperature. The electrochemical tests were performed between 3–1 V vs. Li^+/Li and C-rate currents applied were calculated based on anatase TiO_2 theoretical capacity of 168 mAh g^{-1}.

3. Results and discussion

The schematic diagram of synthetic process of CNT@mesoporous TiO_2 hybrid nanocables is illustrated in Fig. 1 (top panel). Firstly, CNTs were treated with concentrated nitric acid to introduce some functional oxygenated groups (step 1). During the sol–gel process, amorphous TiO_2 layer was uniformly deposited on CNTs by the hydrolysis of TBOT in the

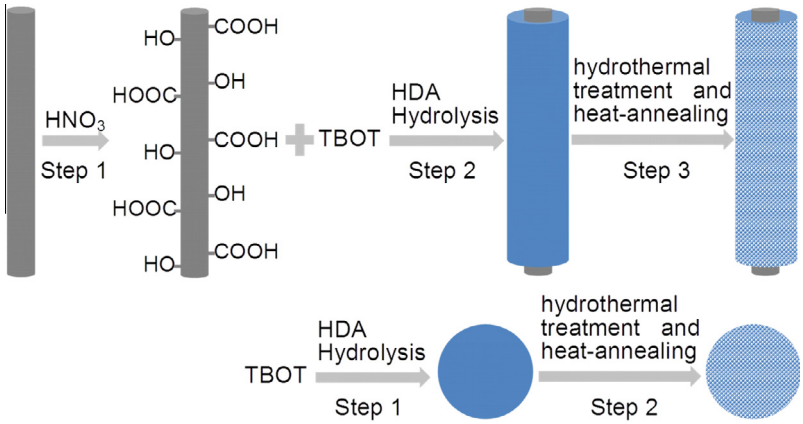

Fig. 1 – Schematic diagram of the synthetic processes of (top panel) CNT@mesoporous TiO_2 hybrid nanocables and (bottom panel) reference TiO_2 spheres without CNT. (A color version of this figure can be viewed online.)

presence of HDA (step 2). Finally, the deposited amorphous TiO_2 was crystallized to form mesoporous-structured TiO_2 via a hydrothermal treatment and heat-annealing (step 3). Without CNT, a control experiment was also carried out followed the same experiment procedure and TiO_2 spheres were obtained (bottom panel). This result strongly suggests that CNTs play the role as templates in the synthesis of the hybrid nanocables.

According to previous reports, the hydrolysis of organic titanate could also produce porous TiO_2 layer on CNTs, but the experiment condition needed to be well controlled to achieve proper hydrolysis rate and kinetics [40,41]. The developed strategy is different from the controlled hydrolysis method. Herein, HDA as a structure directing agent is used for the assembly of porous TiO_2 on CNTs [42]. If there was no HDA added during the hydrolysis, a composite of separated CNT with seriously aggregated TiO_2 particles were formed (shown in Supporting information Figure S1). On the basis of the above results, a possible formation process was proposed: In the mixture, HDA was likely to adsorb on the surface of CNTs by the interaction with the oxygenated groups. During the sol–gel process, titanium species/oligomers was continuously generated from the hydrolysis of TBOT and assembled around the HDA to form porous structure depositing on CNTs. Therefore, there is less special requirement in controlling the experiment condition in this new method.

The crystal structure of CNT@mesoporous TiO_2 hybrid nanocables was analyzed by using XRD and Raman spectroscopy, yielding the results shown in Fig. 2. All the diffraction peaks in the XRD pattern of the hybrid nanocables (Fig. 2A curve a) can be perfectly assigned to anatase TiO_2 (JCPDS card No. 21-1272). No characteristic diffraction peak of CNT appeared, indicating its low content in the hybrid and the thick sheath on its surface. Fig. 2B shows the corresponding Raman spectrum of CNT@mesoporous TiO_2 hybrid nanocables and CNT. In curve a, four Raman modes with strong intensities at 149, 391, 509, and 627 cm^{-1} are consistent with the typical Raman features of anatase TiO_2 phase [43]. Meanwhile, strong D band and G band are observed, verifying the existence of CNTs in the hybrid, and their slight shift towards low frequency may be caused by the interaction of TiO_2 with

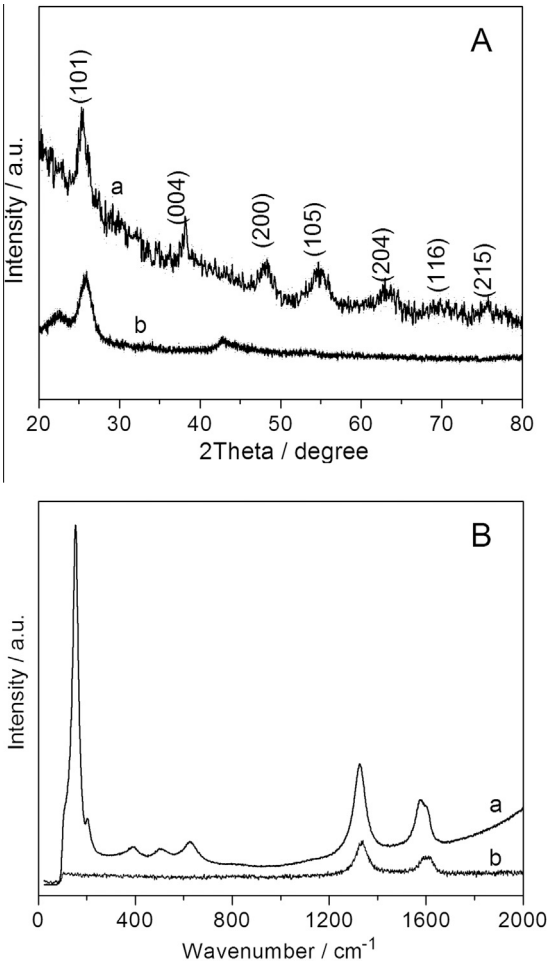

Fig. 2 – (A) Typical XRD patterns and (B) Raman spectra of (a) CNT@mesoporous TiO_2 hybrid nanocables and (b) CNT.

CNT. TGA was carried out to evaluate the weight ratio of the hybrid. The weight loss at below 100 °C is mainly due to the dehydration. The result indicates that the hybrid contains 82.5% TiO_2, 15.5% CNT and 2% H_2O (shown in Supporting information Figure S2).

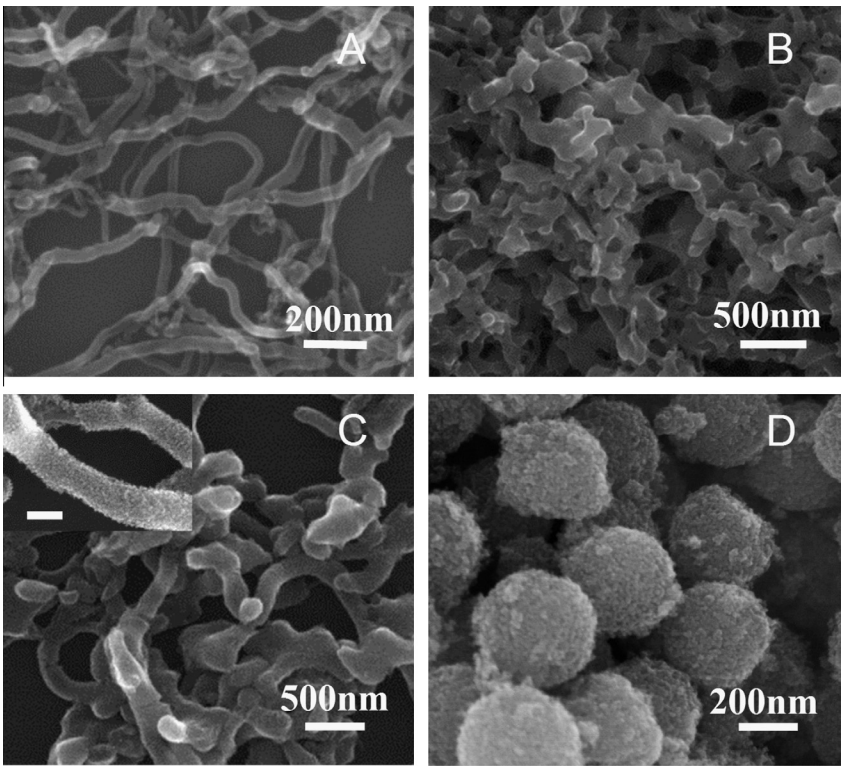

Fig. 3 – SEM images of (A) acid-treated CNTs, (B) amorphous TiO_2 deposited on CNTs, (C) CNT@mesoporous TiO_2 hybrid nanocables, and (D) reference TiO_2 spheres. The inset in (C) is the enlarged SEM image of CNT@mesoporous TiO_2 hybrid nanocables, and the scale bar is 200 nm.

Fig. 3 displays the SEM images of CNT@mesoporous TiO_2 hybrid nanocables. Fig. 3A presents the image of functionalized CNTs with an outer diameter of approximately 40–70 nm (TEM image shown in Supporting information Figure S3). The aggregation of CNTs can be retarded by coating them with amorphous TiO_2, and the resultant composite is shown in Fig. 3B. After the hydrothermal and heat treatment, CNT@mesoporous TiO_2 hybrid was produced. Fig. 3C shows that the hybrid mainly consists of 1D nanostructures interlocking with each other. Neither assemblies of CNT-TiO_2 without CNT support nor bare CNT are found in the sample. The 1D nanostructures appear to have rough surfaces with an average diameter of about 200 nm, whereas the acid-treated CNTs have a smaller diameter. It indicates that the TiO_2 layer has been successfully coated on CNTs. Further evidence can be found from the closer SEM image. A uniform coating layer of numerous nanoparticles on the nanocable surface can be clearly seen in the inset. Without CNT, TiO_2 spheres composed of nanoparticles are obtained, which is consistent with the previous report [42]. Fig. 3D shows the diameter of the spheres is 300–400 nm.

To further examine the architecture of CNT@mesoporous TiO_2 hybrid, TEM and HRTEM were performed. Fig. 4A reveals that the hybrid is composed of 1D nanocables with diameter ranging from 150 to 200 nm, which is significantly larger that of acid-treated CNTs. Accordingly, the thickness of TiO_2 sheath could be about 40–70 nm by estimation. As it shown in Fig. 4B, the porous sheath with small pores comprising numerous highly interconnected nanoparticles was covered on the CNT backbone. It needs to point out that compared with a dense TiO_2 sheath, the porous ones can increase the electrolyte/electrode contact area and perfectly facilitate the transportation of lithium ions, which is critical for high-rate LIB applications. Meanwhile, the underneath conductive CNT would benefit the fast electron transfer. Fig. 4C shows a TEM image of a broken nanocable. It reveals the core/sheath structure of the hybrid nanocable. A uniform sheath with a thickness of about 45 nm is coated on the surface of a CNT. The nanoparticles are estimated to be about 6–14 nm. The HRTEM image in Fig. 4D confirms the small nanoparticles are nanocrystalline TiO_2. The lattice fringes are clearly visible with an interplanar spacing of 0.35 nm, which agrees well with the d_{101} spacing of anatase TiO_2.

The highly porous structure of as-synthesized CNT@mesoporous TiO_2 hybrid nanocables is further confirmed by N_2 adsorption/desorption measurements with the resultant isotherms shown in Fig. 5. The CNT@mesoporous TiO_2 hybrid nanocables and reference TiO_2 exhibit a similar isotherm pattern, which could be approximately categorized to type IV with a H3 hysteresis loop, indicating the presence of a mesoporous structure within the two samples. Based on the BET analysis, the hybrid nanocables show a total specific surface area of 110.9 $m^2 g^{-1}$, which is larger than that of TiO_2 spheres (90.5 $m^2 g^{-1}$). The Barrett–Joyner–Halenda (BJH) pore size distribution (inset) indicates that the pores within CNT@mesoporous TiO_2 nanocables and mesoporous TiO_2 spheres have a similar size of around 8 nm.

To evaluate the lithium storage capabilities of CNT@mesoporous TiO_2 hybrid nanocables, a series of chemical measurements were carried out. Fig. 6A depicts the charge/discharge

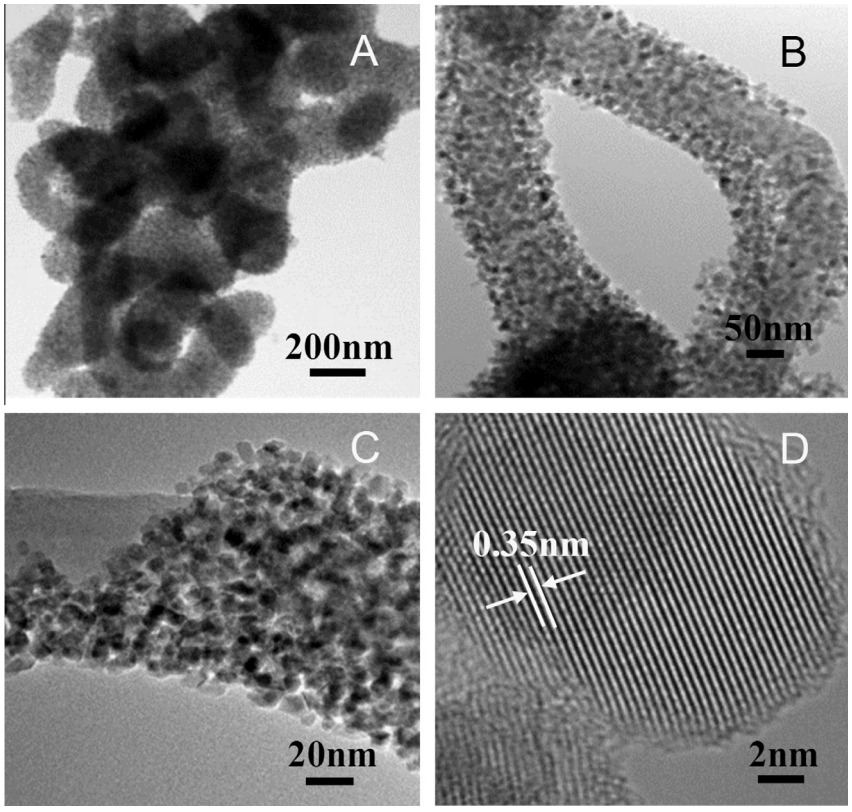

Fig. 4 – TEM images (A–C) and HRTEM image (D) of CNT@mesoporous TiO_2 hybrid nanocables.

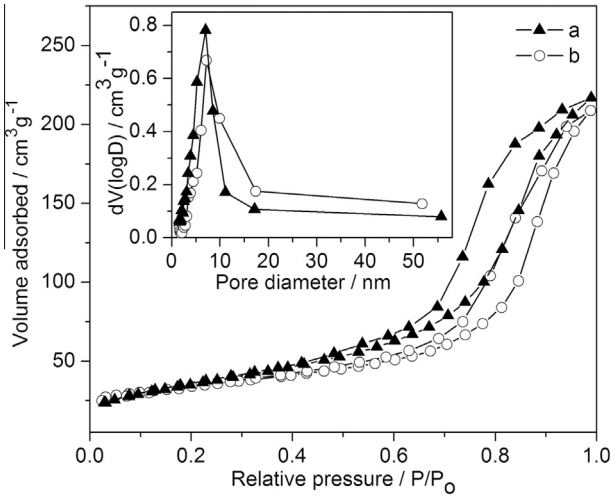

Fig. 5 – Nitrogen isotherm adsorption–desorption curves of (a) CNT@mesoporous TiO_2 hybrid nanocables and (b) reference TiO_2 spheres. The inset is BJH pore size distribution of (a) and (b).

voltage profiles at a current rate of 0.1C. Two voltage plateaus are observed at about 1.77 and 1.87 V during the discharge and charge process, respectively, which is consistent with that reported for anatase TiO_2 [17]. The rate capability test results are shown in Fig. 6B. The CNT@ mesoporous TiO_2 nanocables electrode shows a specific capacity of 183 mAh g^{-1} at 1C, which is higher than the theoretical value (168 mAh g^{-1}) of anatase TiO_2 at 1C. To identify the capacity contribution from CNTs, Li^+ insertion/extraction behavior of the CNTs was also studied (shown in Supporting information Figure S4) in the voltage range of 1–3 V. For 12% CNT in the hybrid, capacity contribution from CNTs can be estimated to 0.6 mAh g^{-1}, which is negligible. The same conclusion has also been pointed out by other research previously [44,45]. Considering the negligible capacity contribution of CNT, we assume that such a high capacity of the hybrid nanocables could be attributed to its unique structure and nanoscale dimension of TiO_2. Compared with the reference TiO_2 spheres, the CNT@mesoporous TiO_2 hybrid nanocables electrode exhibits a better rate performance at various rates from 0.1C to 10C. For example, the hybrid nanocable electrode delivers discharge capacity of 210 mAh g^{-1} at 0.5C, 137 mAh g^{-1} at 5C, and 112 mAh g^{-1} at 10C, whereas the values for TiO_2 spheres are 162 mAh g^{-1}, 98 mAh g^{-1}, and 78 mAh g^{-1}, respectively. The striking contrast demonstrates the efficiency of our protocol to improve the electrochemical performance of TiO_2 by incorporation of CNT within each nanocable. Importantly, after the thirty cycles tested under different current densities even up to 10C, a stable specific capacity of the hybrid nanocables can recover its initial value, indicating the high reversibility of lithium ion insertion/extraction in the electrode. Fig. 6C shows the cycling performance of CNT@mesoporous TiO_2 hybrid nanocables at current rates of 1C and 10C. It demonstrates a stable cycling performance with reversible capacities of 183 mAh g^{-1} (1C) and 112 mAh g^{-1} (10C) retained after 70 cycles. Obviously, the excellent rate-performance of the hybrid nanocables is

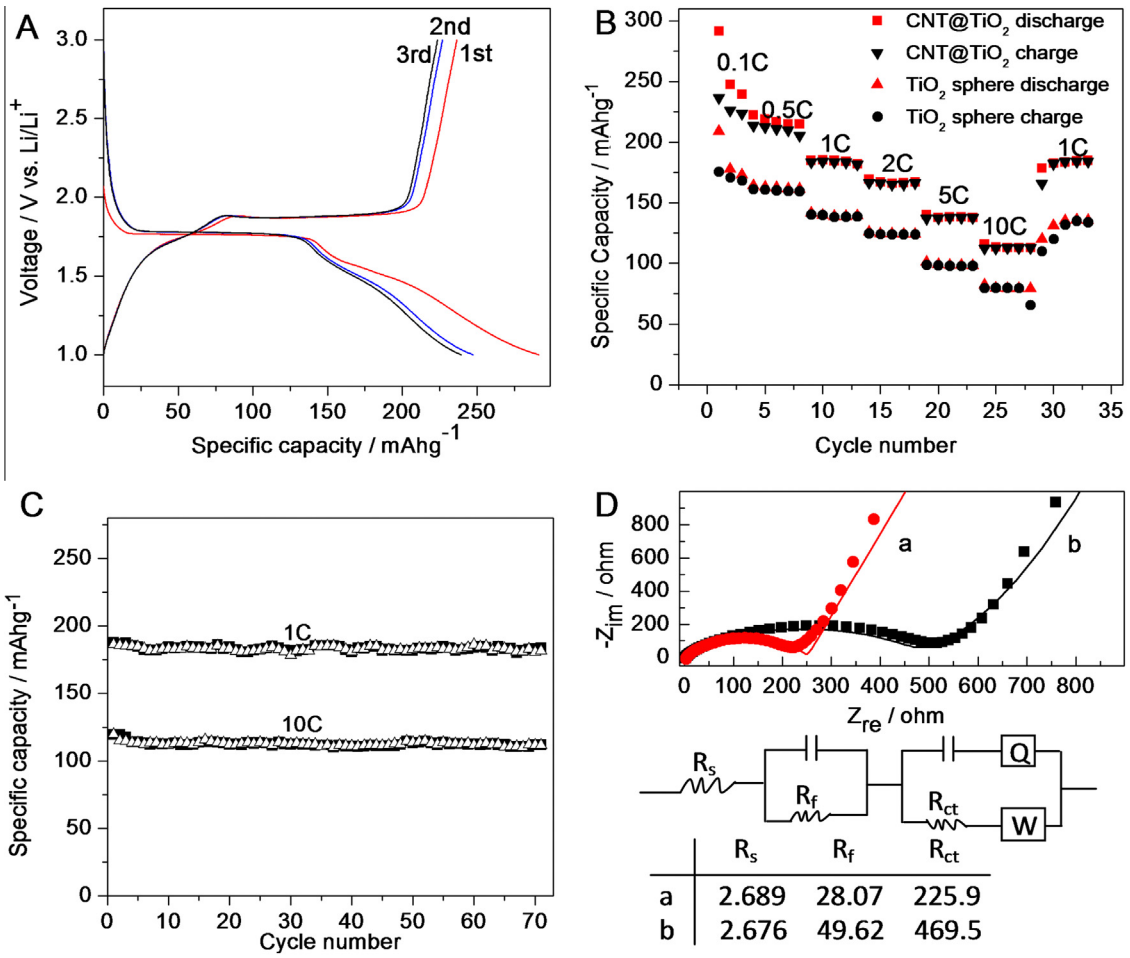

Fig. 6 – Electrochemical measurements of samples. (A) First three charge–discharge voltage profiles of CNT@ mesoporous TiO_2 hybrid nanocables at a current rate of 0.1 C. (B) Specific capacity performance of CNT@ mesoporous TiO_2 hybrid nanocables and reference TO_2 spheres at different current rates from 0.1 C to 10 C. (C) Cycling performance of CNT@ mesoporous TiO_2 hybrid nanocables at constant current rates of 1 C and 10 C. (D) Nyquist plots of CNT@ mesoporous TiO_2 hybrid nanocables (a) and reference TO_2 spheres (b) obtained by applying a sine wave with amplitude of 5.0 mV over the frequency range from 100 kHz to 0.01 Hz, the equivalent electrical circuit and the fitted impedance parameters (Ω). (A color version of this figure can be viewed online.)

better than that of some reported TiO_2-based nanomaterials, such as anatase TiO_2 nanoparticles/beads/nanowires, and TiO_2-graphene composite nanofibers [17,19,46,47].

Three reasons are suggested for the improved capacity and rate performance of CNT@mesoporous TiO_2 hybrid nanocables. Firstly, the mesoporous structure of TiO_2 sheath with larger surface area facilitates the fast penetration of lithium ions and diffusion of electrolytes so that the specific capacity and rate capability can be substantially improved. Another reason is attributed to the increase in electronic conductivity. Fig. 6D compares the Nyquist plots of electrodes of CNT@mesoporous TiO_2 hybrid nanocables and reference TiO_2 spheres, and the data have been analyzed by fitting to an equivalent electrical circuit shown in Fig. 6D. This equivalent circuit model contains R_s related to Li^+ transport resistance in the electrolyte, R_f and a capacitance (C) corresponding to Li^+ migration resistance through the multilayer surface films, R_{ct} and a constant phase element (CPE) related to the charge transfer resistance through the electrode–electrolyte interface and a Warburg impedance (W) associated with Li^+ diffusion in TiO_2 particles. The fitted impedance parameters are listed in Fig. 6D. Due to the same assembly components and condition, the R_s values for both two samples are almost the same. However, the R_f and R_{ct} values are different, especially the R_{ct} value of the hybrid electrode is much smaller than that of TiO_2 spheres. This can be attributed to the electronically conductive CNT core that improves the high conductivity of the hybrid electrode. The increased conductivity benefits the charge transfer, leading to better high-rate performance. Moreover, CNT within each nanocable can act as a mini-current collector, which is also favorable for the fast electron transfer. Thirdly, the unique structure of the hybrid nanocables has advantages in providing easier Li^+ ions permission and transport pathway, thus increase the rate capability. As revealed in Fig. 6B, even at slow charge/discharge rates, the hybrid nanocables shows a higher capacity than that of TiO_2 spheres. The similar phenomenon was also reported by other group [48]. Herein, we

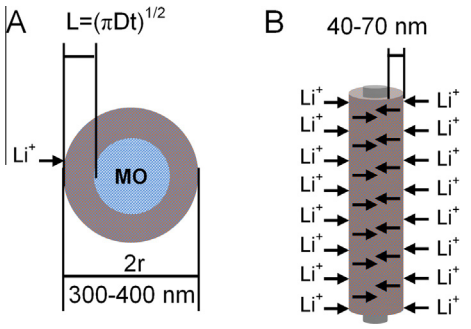

Fig. 7 – (A) A schematic representation of the effective diffusion length in TiO_2 spheres electrode. The area marked in brown shows the volume reacting with Li^+ ions in the charge/discharge period t in a diffusion-controlled process. (B) A schematic representation of the reduced diffusion length in CNT@mesoporous TiO_2 hybrid nanocable. (A color version of this figure can be viewed online.)

contribute it to the special structure of the hybrid. Fig. 7 shows schematic presentation of the electrochemical reaction path on hybrid nanocables and TiO_2 spheres electrodes, respectively. The diffusion rate for Li^+ ions can be estimated based on a diffusion equation relating to two-dimensional Brownian motion, $L = (\pi Dt)^{1/2}$, where L is the diffusion distance, D is the diffusion coefficient, and t is time [49]. The TiO_2 spheres with larger size of 300–400 nm tend to lower the kinetics of diffusion. As a result, polarization is increased during the charge and discharge, which results in the poor charge-rate and discharge-rate capability. In contrast, mesoporous TiO_2 sheath coated on CNTs with thickness of 40–70 nm can be easily filled with electrolyte solution to provide shorter Li^+ ions transport pathways throughout the material, increasing the utilization of TiO_2 crystallites. Furthermore, the higher surface area of the hybrids reduces the effective specific current density, thus improve the rate capability. As a result, the hybrid also demonstrated a significant improvement in specific energy capacities at high charge/discharge rates.

4. Conclusion

In summary, we have demonstrated an efficient fabrication of CNT@mesoporous TiO_2 hybrid nanocables. By using CNTs as templates, mesoporous TiO_2 composed of numerous densely packed nanoparticles was deposited on its surface and the thickness was estimated to be 40–70 nm. The prepared CNT@mesoporous TiO_2 nanocables with unique advantages of porosity, 1D nanostructure, large surface area and higher conductivity shows excellent cycling stability and rate performance. In addition to its promising application for high-power LIBs, the CNT@mesoporous TiO_2 hybrid nanocables are anticipated to have other applications including photocatalysis and dye-sensitized solar cells.

Acknowledgements

This work was supported by National Natural Science Foundation of China (NSFC Grant 21205120) and Research Grants Council of the Hong Kong Administrative Region, China (Project No. CityU 102010).

Appendix A. Supplementary data

Supplementary data associated with this article can be found, in the online version, at http://dx.doi.org/10.1016/j.carbon.2014.04.013.

REFERENCES

[1] Jiang GD, Lin ZF, Zhu LH, Ding YB, Tang HQ. Preparation and photoelectrocatalytic properties of titania/carbon nanotube composite films. Carbon 2010;48(12):3369–75.
[2] Ding SN, Gao BH, Shan D, Sun YM, Cosnier S. TiO_2 nanocrystals electrochemiluminescence quenching by biological enlarged nanogold particles and its application for biosensing. Biosens Bioelectron 2013;39(1):342–5.
[3] Roy P, Kim D, Lee K, Spiecker E, Schmuki P. TiO_2 nanotubes and their application in dye-sensitized solar cells. Nanoscale 2010;2(1):45–59.
[4] Bavykin DV, Friedrich JM, Walsh FC. Protonated titanates and TiO_2 nanostructured materials: synthesis, properties, and applications. Adv Mater 2006;18(21):2807–24.
[5] Bryan JD, Heald SM, Chambers SA, Gamelin DR. Strong room-temperature ferromagnetism in Co^{2+}-doped TiO_2 made from colloidal nanocrystals. J Am Chem Soc 2004;126(37):11640–7.
[6] Guo YG, Hu YS, Sigle W, Maier J. Superior electrode performance of nanostructured mesoporous TiO_2 (anatase) through efficient hierarchical mixed conducting networks. Adv Mater 2007;19(16):2087–91.
[7] Zhao L, Hu YS, Li H, Wang ZX, Chen LQ. Porous $Li_4Ti_5O_{12}$ coated with N-doped carbon from ionic liquids for Li-ion batteries. Adv Mater 2011;23(11):1385–8.
[8] Liu JH, Chen JS, Wei XF, Lou XW, Liu XW. Sandwich-like, stacked ultrathin titanate nanosheets for ultrafast lithium storage. Adv Mater 2011;23(8):998–1002.
[9] Hu YS, Kienle L, Guo YG, Maier J. High lithium electroactivity of nanometer-sized rutile TiO_2. Adv Mater 2006;18(11):1421–6.
[10] Jiang CH, Wei MD, Qi ZM, Kudo T, Honma I, Zhou HS. Particle size dependence of the lithium storage capability and high rate performance of nanocrystalline anatase TiO_2 electrode. J Power Sources 2007;166(1):239–43.
[11] Joo JB, Dahl M, Li N, Zaera F, Yin YD. Tailored synthesis of mesoporous TiO_2 hollow nanostructures for catalytic applications. Energy Environ Sci 2013;6(7):2082–92.
[12] Kowalski D, Kim D, Schmuki P. TiO_2 nanotubes, nanochannels and mesosponge: self-organized formation and applications. Nano Today 2013;8(3):235–64.
[13] Maier J. Nanoionics: ion transport and electrochemical storage in confined systems. Nat Mater 2005;4(11):805–15.
[14] Liu ZL, Hong L, Guo B. Physicochemical and electrochemical characterization of anatase titanium dioxide nanoparticles. J Power Sources 2005;143(1–2):231–5.
[15] Tang YP, Tan XX, Hou GY, Cao HZ, Zheng GQ. Synthesis of dense nanocavities inside TiO_2 nanowire array and its electrochemical properties as a three-dimensional anode material for Li-ion batteries. Electrochim Acta 2012;78:154–9.
[16] Kyerematen NA, Plylahan N, dos Santos ACS, Taveira LV, Dick LFP, Djenizian T. Sulfidated TiO_2 nanotubes: a potential 3D cathode material for Li-ion micro batteries. Chem Commun 2013;49(39):4205–7.

[17] Saravanan K, Ananthanarayanan K, Balaya P. Mesoporous TiO_2 with high packing density for superior lithium storage. Energy Environ Sci 2010;3(7):939–48.
[18] Anh V, Qian YQ, Stein A. Porous electrode materials for lithium-ion batteries – how to prepare them and what makes them special. Adv Energy Mater 2012;2(9):1056–85.
[19] Zhu KL, Tian JH, Liu YP, Lin N, Tang QW, Yu XM, et al. Submicron-sized mesoporous anatase TiO_2 beads with a high specific surface synthesized by controlling reaction conditions for high-performance Li-batteries. RSC Adv 2013;3(32):13149–55.
[20] Liu HS, Bi ZH, Sun XG, Unocic RR, Paranthaman MP, Dai S, et al. Mesoporous TiO_2-B microspheres with superior rate performance for lithium ion batteries. Adv Mater 2011;23(30):3450–4.
[21] Wang J, Zhou YK, Hu YY, O'Hayre R, Shao ZP. Facile synthesis of nanocrystalline TiO_2 mesoporous microspheres for lithium-ion batteries. J Phys Chem C 2011;115(5):2529–36.
[22] Nam SH, Shim HS, Kim YS, Dar MA, Kim JG, Kim WB. Ag or Au nanoparticle-embedded one-dimensional composite TiO_2 nanofibers prepared via electrospinning for use in lithium-ion batteries. ACS Appl Mater Inter 2010;2(7):2046–52.
[23] Chang PY, Huang CH, Doong RA. Ordered mesoporous carbon-TiO_2 materials for improved electrochemical performance of lithium ion battery. Carbon 2012;50(11):4259–68.
[24] Wang WS, Sa QN, Chen JH, Wang Y, Jung HJ, Yin YD. Porous TiO_2/C nanocomposite shells as a high-performance anode material for lithium-ion batteries. ACS Appl Mater Inter 2013;5(14):6478–83.
[25] Baughman RH, Zakhidov AA, de Heer WA. Carbon nanotubes – the route toward applications. Science 2002;297(5582):787–92.
[26] Dresselhaus MS, Dresselhaus G, Saito R. Physics of carbon nanotubes. Carbon 1995;33(7):883–91.
[27] Jegal JP, Kim KB. Carbon nanotube-embedding $LiFePO_4$ as a cathode material for high rate lithium ion batteries. J Power Sources 2013;243:859–64.
[28] Noerochim L, Wang JZ, Chou SL, Wexler D, Liu HK. Free-standing single-walled carbon nanotube/SnO_2 anode paper for flexible lithium-ion batteries. Carbon 2012;50(3):1289–97.
[29] Chen WX, Lee JY, Liu ZL. The nanocomposites of carbon nanotube with Sb and $SnSb_{0.5}$ as Li-ion battery anodes. Carbon 2003;41(5):959–66.
[30] Seo SG, Nam WH, Lim YS, Seo WS, Cho YS, Lee YJ. Temperature-dependent charge transport in TiO_2–multiwalled carbon nanotube composites. Carbon 2014;67:688–93.
[31] Khalilian M, Abdi Y, Arzi E. Formation of well-packed TiO_2 nanoparticles on multiwall carbon nanotubes using CVD method to fabricate high sensitive gas sensors. J Nanopart Res 2011;13(10):5257–64.
[32] Zhu PN, Wu YZ, Reddy MV, Nair AS, Chowdari BVR, Ramakrishna S. Long term cycling studies of electrospun TiO_2 nanostructures and their composites with MWCNTs for rechargeable Li-ion batteries. RSC Adv 2012;2(2):531–7.
[33] Yang MQ, Zhang N, Xu YJ. Synthesis of fullerene-, carbon nanotube-, and graphene-TiO_2 nanocomposite photocatalysts for selective oxidation: a comparative study. ACS Appl Mater Inter 2013;5(3):1156–64.
[34] Wang HH, Dong SJ, Chang Y, Faria JL. Enhancing the photocatalytic properties of TiO_2 by coupling with carbon nanotubes and supporting gold. J Hazard Mater 2012;235:230–6.
[35] Li ZY, Gao B, Chen GZ, Mokaya R, Sotiropoulos S, Puma GL. Carbon nanotube/titanium dioxide (CNT/TiO_2) core-shell nanocomposites with tailored shell thickness, CNT content and photocatalytic/photoelectrocatalytic properties. Appl Catal B – Environ 2011;110:50–7.
[36] Jitianu A, Cacciaguerra T, Benoit R, Delpeux S, Beguin F, Bonnamy S. Synthesis and characterization of carbon nanotubes–TiO_2 nanocomposites. Carbon 2004;42(5–6):1147–51.
[37] Eder D, Windle AH. Carbon-inorganic hybrid materials: the carbon-nanotube/TiO_2 interface. Adv Mater 2008;20(9):1787–93.
[38] Zhou HJ, Liu L, Wang XC, Liang FX, Bao SJ, Lv DM, et al. Multimodal porous CNT@TiO_2 nanocables with superior performance in lithium-ion batteries. J Mater Chem A 2013;1(30):8525–8.
[39] Takenaka S, Arike T, Matsune H, Kishida M. Coverage of carbon nanotubes with titania nanoparticles for the preparation of active titania-based photocatalysts. Appl Catal B – Environ 2012;125:358–66.
[40] Cao FF, Guo YG, Zheng SF, Wu XL, Jiang LY, Bi RR, et al. Symbiotic coaxial nanocables: facile synthesis and an efficient and elegant morphological solution to the lithium storage problem. Chem Mater 2010;22(5):1908–14.
[41] Liu B, Zeng HC. Carbon nanotubes supported mesoporous mesocrystals of anatase TiO_2. Chem Mater 2008;20(8):2711–8.
[42] Chen DH, Cao L, Huang FZ, Imperia P, Cheng YB, Caruso RA. Synthesis of monodisperse mesoporous titania beads with controllable diameter, high surface areas, and variable pore diameters (14–23 nm). J Am Chem Soc 2010;132(12):4438–44.
[43] Wang ZW, Saxena SK. Raman spectroscopic study on pressure-induced amorphization in nanocrystalline anatase (TiO_2). Solid State Commun 2001;118(2):75–8.
[44] Ding SJ, Chen JS, Lou XW. One-dimensional hierarchical structures composed of novel metal oxide nanosheets on a carbon nanotube backbone and their lithium-storage properties. Adv Funct Mater 2011;21:4120–5.
[45] Wu BH, Lou XW, Hng HH. Titania nanosheets hierarchically assembled on carbon nanotubes as high-rate anodes for lithium-ion batteries. Chem Eur J 2012;18:3132–5.
[46] Wang HE, Lu ZG, Xi LJ, Ma RG, Wang CD, Zapien JA, et al. Facile and rapid synthesis of highly porous wirelike TiO_2 as anodes for lithium-ion batteries. ACS Appl Mater Inter 2012;4(3):1608–13.
[47] Zhang X, Kumar PS, Aravindan V, Liu HH, Sundaramurthy J, Mhaisalkar SG, et al. Electrospun TiO_2-graphene composite nanofibers as a highly durable insertion anode for lithium ion batteries. J Phys Chem C 2012;116(28):14780–8.
[48] Shen LF, Yuan CZ, Luo HJ, Zhang XG, Xu K, Zhang F. In situ growth of $Li_4Ti_5O_{12}$ on multi-walled carbon nanotubes: novel coaxial nanocables for high rate lithium ion batteries. J Mater Chem 2011;21:761–7.
[49] Zhou HS, Li DL, Hibino M, Honma I. A self-ordered, crystalline-glass, mesoporous nanocomposite for use as a lithium-based storage device with both high power and high energy densities. Angew Chem Int Ed 2005;44:797–802.